Insights into S100 Target Specificity Examined by a New Interaction between S100A11 and Annexin A2†

Anne C. Rintala-Dempsey, Liliana Santamaria-Kisiel, Yinyin Liao, Gilles Lajoie, and Gary S. Shaw*

Department of Biochemistry, The University of Western Ontario, London, Ontario, Canada N6A 5C1

Received August 25, 2006; Revised Manuscript Received October 5, 2006

ABSTRACT: S100 proteins are a group of EF-hand calcium-signaling proteins, many of which interact with members of the calcium- and phospholipid-binding annexin family of proteins. This calcium-sensitive interaction enables two neighboring membrane surfaces, complexed to different annexin proteins, to be brought into close proximity for membrane reorganization, using the S100 protein as a bridging molecule. S100A11 and S100A10 are two members of the S100 family found to interact with the N-termini of annexins A1 and A2, respectively. Despite the high degree of structural similarity between these two complexes and the sequences of the peptides, earlier studies have shown that there is little or no cross-reactivity between these two S100s and the annexin peptides. In the current work the specificity and the affinity of the interaction of the N-terminal sequences of annexins A1 and A2 with Ca^{2+}-S100A11 were investigated. Through the use of alanine-scanning peptide array experiments and NMR spectroscopy, an approximate 5-fold tighter interaction was identified between Ca^{2+}-S100A11 and annexin A2 ($\sim$3 μM) compared to annexin A1 ($\sim$15 μM). Chemical shift mapping revealed that the binding site for annexin A2 on S100A11 was similar to that observed for the annexin A1 but with distinct differences involving the C-terminus of the annexin A2 peptide. In addition, kinetic measurements based on NMR titration data showed that annexin A2 binding to Ca^{2+}-S100A11 occurs at a comparable rate ($\sim$120 s^{-1}) to that observed for membrane fusion processes such as endo- and exocytosis.

The S100 proteins are a group of EF-hand calcium-binding proteins involved in diverse calcium-signaling events such as regulation of protein phosphorylation, modulation of enzymatic activity, and cytoskeletal dynamics (*1*, *2*). They are small, dimeric, α-helical proteins with each monomer consisting of a pair of EF-hand calcium-binding motifs. Structures of calcium-free and calcium-bound forms of several S100 proteins have shown that a rearrangement of the helices within each monomer exposes a hydrophobic patch on each side of the dimer, making interaction with two target molecules possible. The broad, shallow surface of this hydrophobic patch allows some of the S100 proteins, such as S100B, S100A1, and S100A6, to form complexes with as many as 20 different target proteins (*2*−*4*). In this manner the specificity of the S100 proteins parallels another calcium-binding protein, calmodulin, although they differ significantly in their target proteins and modes for protein recognition. To date, a variety of studies have shown that several S100 proteins interact with members of the annexin family of calcium- and phospholipid-binding proteins. For this tetrameric complex, the S100 dimer acts as a bridge between two annexin molecules (*5*) utilizing the N-terminal sequences of each annexin protein. This mechanism enables two neighboring membrane surfaces to be brought into close proximity for membrane reorganization in processes such as vesiculation. For example, the complex between S100A10 and annexin A2 is involved in the distribution and fusion processes of early endosomes (*6*, *7*), and a similar role has been proposed for the Ca^{2+}-S100A11/annexin A1 complex (*8*). In some cases an S100 protein can interact with several members of the annexin family. In this manner, S100A6 has been shown to interact with annexins A2 (*9*−*11*), A5 (*10*), A6 (*9*), and A11 (*10*, *12*−*16*). In other cases a single annexin can interact with several S100 family members. Thus, annexin A2 can form complexes with S100A4 (*17*), S100A6 (*9*), and S100A10 (*18*−*29*). These observations raise many intriguing questions regarding the S100−annexin specificity, binding affinity, and recognition. For example, how does the hydrophobic surface on the S100 protein recognize some annexin proteins while excluding others? How do the similarities and differences between the N-terminal sequences of the annexins result in differences in interactions and affinity for specific members of the S100 family?

Initial insights into the specificity of the S100−annexin interaction have been provided by the crystal structures of S100A10 and Ca^{2+}-S100A11[1] in complex with the N-terminal regions of annexin A2 (*18*) and annexin A1 (*30*), respectively. These two structures are very similar to each other, in terms of both the folds of the proteins and the secondary structure and binding locations of the annexin

† This work was supported by funding from the Canadian Institutes of Health Research (G.S.S.) and the Natural Sciences and Engineering Research Council (G.L.) and an award from the Canada Research Chairs Program (G.S.S.).

* Author to whom correspondence should be addressed. Phone: 519-661-4021. Fax: 519-661-3175. E-mail: gshaw1@uwo.ca. Web: www.biochem.uwo.ca/fac/shaw.

[1] Abbreviations: Ca^{2+}-S100A11, calcium-bound S100A11 protein; RMSD, root mean square deviation; Fmoc, fluorenylmethyloxycarbonyl; GST, glutathione *S*-transferase; DTT, dithiothreitol.

10.1021/bi061754e CCC: $33.50
Published on Web 11/15/2006

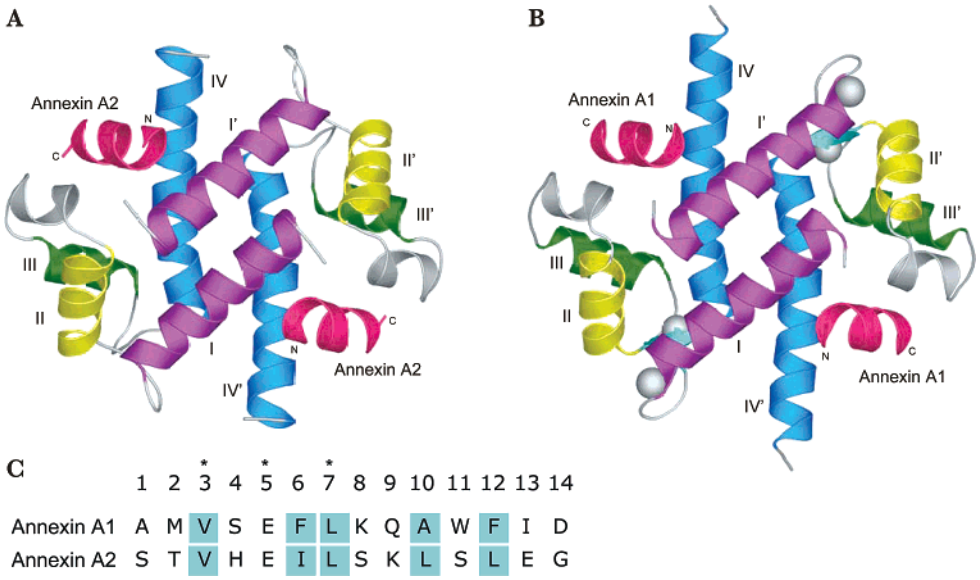

FIGURE 1: Structural similarity of S100A10 and S100A11 in complex with annexin target peptides. (A) Ribbon representation of the structure of apo-S100A10 bound to the N-terminal peptide of annexin A2 (*18*). The helices of the protein are numbered I−IV for one monomer and I′−IV′ for the second monomer. Two annexin A2 peptides (shown in pink) interact with the S100A10 dimer, bridging the two monomers. The N-terminus of the peptide makes contacts with helix I′ of one monomer while the remainder of the peptide interacts with the linker and helices III and IV of the other monomer. (B) Ribbon representation of the structure of Ca^{2+}-S100A11 bound to the N-terminal peptide of annexin A1 (*30*). The annexin A1 peptide interacts with the Ca^{2+}-S100A11 dimer in a similar manner to the annexin A2 peptide interaction with S100A10. When superimposed, the two structures are virtually identical, having a backbone RMSD of 0.85 Å. (C) Sequence alignment of the N-terminal sequences of annexin A1 and A2. Identical residues are indicated with asterisks, and hydrophobic residues at matching positions are highlighted in cyan.

peptides (Figure 1). Despite these similarities previous fluorescence experiments have shown that annexin A2 does not interact with Ca^{2+}-S100A11, and annexin A1 will not form a complex with S100A10 (*30*, *31*). This proposed specificity is surprising given the multiple interactions of annexin A2 with other S100 proteins (described above). Alternatively, an understanding of the molecular details of the interactions of Ca^{2+}-S100A11 with these annexins might provide a basis for the recognition and specificity of the S100 target protein interaction. In the current study, the specificity and affinities of interaction for the N-terminal sequences of annexins A1 and A2 with Ca^{2+}-S100A11 were investigated. Through the use of peptide array experiments and NMR spectroscopy, a surprisingly strong interaction was found between Ca^{2+}-S100A11 and annexin A2 that was approximately 5-fold tighter than observed for annexin A1. Using chemical shift mapping, the binding site for annexin A2 on S100A11 was found to be similar to that observed for the annexin A1 but with distinct differences involving the C-terminus of the annexin A2 peptide. Further, kinetic measurements using line shape analysis of NMR titration data showed that annexin A2 binding to Ca^{2+}-S100A11 occurs at a comparable rate as observed for membrane fusion events, substantiating a role for this complex in processes such as endo- and exocytosis.

EXPERIMENTAL PROCEDURES

Cloning and Purification of GST-S100A11. The pAED4-S100A11 vector (pET-derived vector) used to express S100A11 for NMR and calorimetry experiments was a generous gift from Dr. Michael Walsh (University of Calgary). To construct GST-tagged S100A11, used for peptide array experiments, the S100A11 sequence was removed from this vector and inserted into a pGEX-6P-1 vector (Amersham) using the *Not*I restriction site. GST-S100A11 was overexpressed in *Escherichia coli* strain BL21-(DE3). The cells were grown in 1 L of 2 × YT medium to an OD_{595} of 0.7, and expression was induced with 0.4 mM IPTG. Cells were harvested, lysed using a French pressure cell, and centrifuged at 38000 rpm for 90 min. The supernatant was applied to a phenyl-Sepharose column in buffer A (25 mM Tris, pH 7.5, 100 mM NaCl, 1 mM DTT, and 5 mM $CaCl_2$) at 4 °C. The GST-S100A11 binds to the column due to a calcium-induced hydrophobic interaction of Ca^{2+}-S100A11 with the phenyl groups. The column was extensively washed with buffer B (25 mM Tris, pH 7.5, 100 mM NaCl, 1 mM DTT, and 1 mM $CaCl_2$) to remove other proteins, and the GST-S100A11 was then eluted by removal of the calcium ions with buffer C (25 mM Tris, pH 7.5, 100 mM NaCl, 1 mM DTT, and 1 mM EGTA). Fractions containing the protein were dialyzed against 50 mM KCl, pH 8.0, and then 3 mM KCl, pH 8.0. The protein was subsequently lyophilized and confirmed by western blot using an anti-GST antibody (Sigma).

Cloning and Purification of S100A11(C9S). Site-directed mutagenesis of S100A11 was performed to replace the cysteine at position 9 with a serine to prevent protein oxidation. The pAED4-S100A11 plasmid was used as the template DNA in the QuikChange site-directed mutagenesis kit (Stratagene). The resulting S100A11(C9S) plasmid was transformed into *E. coli* strain BL21(DE3) for expression. For uniformly ^{15}N-labeled S100A11(C9S), the cells were grown in M9 minimal media with $^{15}NH_4Cl$ as the sole nitrogen source. For ^{13}C,^{15}N-labeled protein, [^{13}C]glucose was used as the sole carbon source. The proteins were expressed and purified as described above for GST-S100A11.

Peptide Array Experiments. Peptides were synthesized on a cellulose membrane using an Auto-Spot Robot ASP 222

(Abimed) based on Fmoc chemistry. Peptides of the wild-type sequences for annexin A1 (AMVSEFLKQAWFID) and annexin A2 (STVHEILSKLSLEG), alanine-scanning mutagenesis of each amino acid in both peptides, and reverse sequences of the annexin A1 and A2 peptides were generated. The C-termini of the peptides were covalently attached to an alanine anchor group on the membrane, and the free N-termini were acetylated using acetic anhydride. After synthesis the dried membrane was first incubated in anhydrous ethanol. Water was gradually added to the membrane to hydrate the peptides and then washed twice in water for 5 min each to remove any residual ethanol; all washes and incubations were performed at room temperature with agitation. The membrane was then washed twice with wash buffer [20 mM Tris-HCl, pH 7.6, 137 mM NaCl, 0.1% (v/v) Tween 20, and 1 mM $CaCl_2$] for 10 min each. The membrane was incubated for 1 h in binding buffer [wash buffer with 5% (w/v) sucrose] with 10 nM GST-S100A11. The binding buffer was removed, and the membrane was rinsed twice with wash buffer and washed twice for 5 min and once for 10 min. The membrane was blocked overnight at 4 °C in blocking buffer (wash buffer with 1% BSA). Rabbit anti-GST antibody (Sigma) was diluted 1:2000 in blocking buffer and incubated with the membrane for 1 h. The membrane was washed as described above and then incubated for 1 h in blocking buffer with anti-rabbit IgG alkaline phosphatase linked antibody diluted by 1:10000. The membrane was washed again as above. Antibodies were detected by ECF reagent as described in the product manual for western blotting (Amersham). Spots were visualized using a Bio-Rad Fluor-S MultiImager at a wavelength setting of 530 nm, an aperture setting of 4, and exposure time of 1.5 s.

Peptide Synthesis. The annexin A1 (AMVSEFLKQAWFIDNEERR) and A2 (STVHEILSKLSLEGD) peptides were synthesized using solid-phase peptide synthesis employing the Fmoc chemistry strategy (*32*). The annexin A1 peptide included a C-terminal NEERR sequence to improve solubility. The N-termini of the peptides were acetylated. Purification by C18 reversed-phase HPLC was followed by lyophilization and verification by mass spectrometry. The calculated molecular masses for the acetylated annexin A1 and A2 peptides were 2411.68 and 1669.81 Da, respectively, and the observed values were 2411.49 and 1668.86 Da.

NMR Spectroscopy. Experiments were performed on a Varian INOVA 600 MHz spectrometer equipped with a pulse field gradient triple resonance probe and collected at 35 °C. All NMR samples contained 10% D_2O, 50 mM KCl, 5 mM DTT, 20 mM MOPS buffer at pH 7.25, and 33 μM DSS as an internal standard. For the NMR sample of apo-S100A11(C9S) the protein concentration was 250 μM (dimer). For the collection of multidimensional NMR experiments, an initial 1 mM apo-S100A11(C9S)(dimer) sample was used after which additions of 10 mM $CaCl_2$ and then 2 mM annexin A2 peptide were made for the calcium- and peptide-bound samples of the protein, respectively. The pH of the sample was adjusted to 7.25 after each addition. To facilitate sequential assignment of the polypeptide backbone, HNCA (*33*, *34*), HNCACB (*35*), and CBCA(CO)NH (*36*) NMR experiments were collected and assigned for the calcium- and peptide-bound forms of the protein. Data was processed using NMRPipe (*37*) and analyzed using NMRView (*38*). Changes in chemical shift were mapped to the surface of Ca^{2+}-S100A11 using MacPyMOL (http://delsci.com/macpymol/).

NMR Titration Experiments. For the titration of Ca^{2+}-S100A11(C9S) with the annexin A2 peptide, an NMR sample of S100A11(C9S) and 5 mM $CaCl_2$ was used. Annexin A2 peptide was added from a stock solution that was prepared by dissolving 1.48 mg of peptide in 500 μL of 4 mM MOPS buffer, pH 7.25, and 10 mM KCl. The peptide solution was adjusted to pH 7 to neutralize the charge and lyophilized. The dried peptide was dissolved in 100 μL of 90% H_2O/10% D_2O with 0.05% sodium azide. Final S100A11(dimer) and annexin A2 concentrations were determined by triplicate amino acid analysis to be 146.5 ± 4.5 μM and 7.6 ± 0.5 mM, respectively, performed at the Alberta Peptide Institute (Edmonton, Alberta, Canada). The peptide was added in 1 or 2 μL increments for 17 additions to a peptide concentration of 368 μM, and a final addition of 8 μL was added to a peptide concentration of 469 μM. The sample was mixed carefully after each addition during the titration and equilibrated for at least 15 min. The total volume increase of the NMR sample was 37 μL (6%). $^1H-^{15}N$ HSQC spectra were collected at each point in the titration, using 1024 complex points in the ^1H dimension and 64 increments in the ^{15}N dimension. Peaks that underwent fast exchange were monitored for change in chemical shift after each addition and fit according to the equation $[PL] = (1/2)\{(P_T + L_T + K_d) - [(P_T + L_T + K_d)^2 - 4P_TL_T]^{1/2}\}$, where [PL] is the concentration of the complex, P_T is the total protein, L_T is the total ligand, and K_d is the dissociation constant. For the intermediate exchange data, the spectra were processed by zero filling to 4096 points in the ^1H dimension and using exponential weighting to produce Lorentzian−Gaussian line shapes. One-dimensional traces through peaks were fit with the line shape equation for two-site exchange described by Hahn, Maxwell, and McConnell (HMM) and Sutherland (*39*−*41*) that describes the off-rate (k_{off}) and dissociation constant as a function of observed chemical shifts and line widths for the free and bound peaks. Both the fast and intermediate exchange data were fit using the global fit option in Prism 4 for Mac OSX (GraphPad Software). For fast exchange data, a shared dissociation constant was determined through fitting of six different data sets to a common curve. For intermediate exchange data, shared values of k_{off}, or k_{off} and K_d, were determined from simultaneous fitting of multiple traces acquired from the titration data.

Isothermal Titration Calorimetry. The association constant of the annexin A1 peptide to Ca^{2+}-S100A11(C9S) was determined by measuring the heat of reaction during the titration of the protein into the peptide solution. The experiments were performed using a Microcal VP-ITC microcalorimeter (Microcal Inc.). For the titration, a sample of 171 μM dimeric Ca^{2+}-S100A11(C9S) in 50 mM Tris, 0.2 mM EDTA, and 5 mM $CaCl_2$ at pH 7.3 was dialyzed for 24 h against 50 mM Tris, 0.2 mM EDTA, 5 mM $CaCl_2$, and 50 mM KCl, pH 7.3, at 4 °C, and the annexin A1 peptide was dissolved in the last dialysis buffer. Protein and peptide solutions were degassed under vacuum prior to each titration. Titrations consisted of 10 μL injections of 171 μM Ca^{2+}-S100A11(C9S)(dimer) into a 1.43 mL cell containing 31 μM annexin A1 peptide. Base line correction was performed by

manually selecting the peak areas for integration. The dissociation constant (K_d) was obtained by fitting the data to a one-site model using Microcal Origin Software. Protein and peptide concentrations were determined by using the content of alanine and leucine from triplicate amino acid analysis performed at the Alberta Peptide Institute (Edmonton, Alberta, Canada).

RESULTS

The three-dimensional structures of N-terminal peptides from different annexin proteins complexed with two different S100 proteins are available (Figure 1). Crystal structures of S100A10 with annexin A2 (*18*) (Figure 1A) and Ca^{2+}-S100A11 with annexin A1 (*30*) (Figure 1B) reveal that the structures, including the annexin peptides, are highly similar to one another, having a backbone RMSD of 0.85 Å. The major difference between these two complexes is that S100A11 is in the calcium-bound state while S100A10 is metal-free due to mutations in both calcium-binding loops that eliminate its ability to bind calcium. Nevertheless, both S100 proteins bind two annexin peptides per dimer, each one interacting with residues in the cleft formed by helices I′, III, and IV and the linker. Further, the annexin peptides form amphipathic helices when in complex and possess three identical residues at positions Val3, Glu5, and Leu7 and conserved hydrophobes at positions Phe/Ile6 and Phe/Leu12. Despite these structural and sequential similarities, it has been observed that the N-terminal annexin A1 peptide does not bind to S100A10 (*30*, *31*) and is specific for S100A11. Thus the S100A10 and S100A11 interactions with the N-terminal regions of annexins A1 and A2 present an ideal model to examine the target specificity and affinities for these S100 proteins.

Binding and Specificity of Annexins A1 and A2 to S100A11. Peptide array experiments were used to examine the interactions between Ca^{2+}-S100A11 and N-terminal peptide sequences of annexin A1 and A2. In this experiment peptides were directly synthesized on a cellulose membrane and then probed with the GST-S100A11 protein in the presence of calcium. Along with wild-type peptide sequences, alanine-scanning mutagenesis of the regions was used to identify important residues in the interactions. Residues that were particularly important for the interaction at the S100A11−peptide interface resulted in diminished binding by Ca^{2+}-S100A11 upon alanine substitution. Peptides were identical lengths and were N-acetylated as this is a requirement for the annexin−S100 interaction (*19*, *26*). Although the GST moiety might potentially interfere with peptide binding, we rationalized this would be a consistent contribution for all peptides studied. Further, the GST was linked to S100A11 by an eight-residue linker that should displace it from any known binding site on S100A11.

The annexin A1 and annexin A2 peptide membranes are shown in Figure 2A, each square containing an individual peptide sequence. Each array was probed with GST-S100A11 in the presence of calcium, and peptide binding was detected using anti-GST and ECF fluorescence. The array shows that the wild-type (WT) sequences of annexin A1 and A2, respectively, both exhibit moderate fluorescence of similar intensity, indicating that Ca^{2+}-S100A11 binds to both annexin A1 and A2 with roughly similar affinities. These spots, or

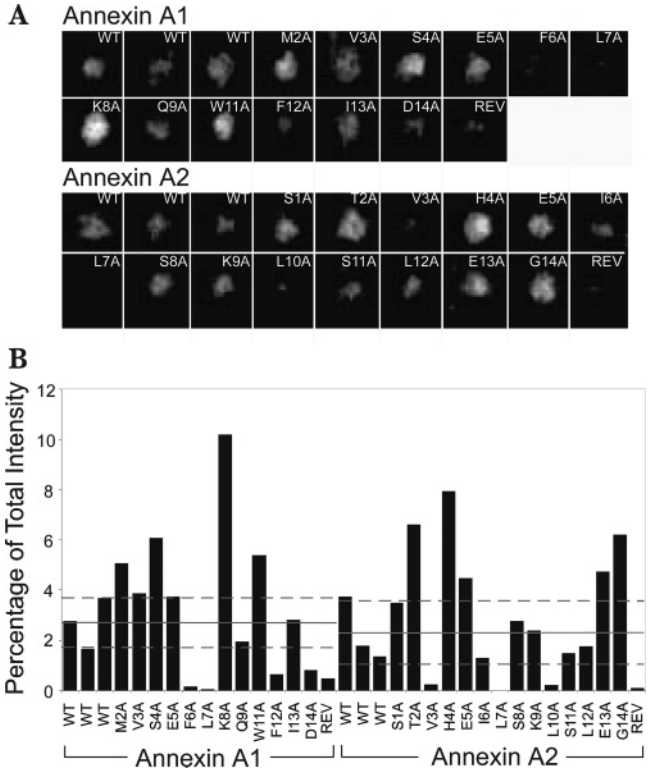

FIGURE 2: Peptide array of annexin A1 and A2 peptides. (A) Representative peptide array of 14-mer sequences from annexins A1 and A2 covalently bound to a cellulose filter. The filter was incubated with 10 nM GST-S100A11(dimer) in the presence of 1 mM $CaCl_2$. Bound protein was detected by anti-GST antibody and chemifluorescence. Alanine scanning mutagenesis was used to generate an array of peptide sequences of annexins A1 (Ac-AMVSEFLKQAWFID) and A2 (Ac-STVHEILSKLSLEG). Each spot is labeled either WT for wild-type sequence, the residue, and position of the alanine mutation or REV for the reverse sequence of the peptide. (B) Histogram of the spot intensities measured using ImageJ software (NIH). Each bar represents the intensity of a given spot as a fraction of the total intensity of all of the spots. The solid gray lines indicate the average intensities, and dotted gray lines are shown at one standard deviation from the average of the WT annexin A1 and A2 peptides at 2.7 ± 1.0 and 2.3 ± 1.3, respectively. These experiments were done in duplicate with similar results (data not shown).

sequences, were repeated in triplicate to give some idea of the variation between peptide spots (indicated by a dashed line in Figure 2B). When comparing binding efficiency, we focused on peptides that provided intensities outside the range exhibited by the wild type (i.e., outside the dashed lines in Figure 2B). In addition, a duplicate peptide array experiment provided nearly identical trends (data not shown). As shown by the last spots in each array, both the annexin A1 and A2 reverse peptide sequences (REV) interacted poorly with the S100A11, indicating the direction of the sequence is critical for correct binding. Compared to the average intensity of the native peptides (WT), the alanine-substituted peptides of both annexin A1 and A2 showed varied degrees of intensity (Figure 2B), indicative of stronger or weaker binding to Ca^{2+}-S100A11, outside the range shown by the wild-type peptide binding. Two peptides from annexin A1 (M2A, S4A) and annexin A2 (T2A, H4A) having alanine substitutions at similar positions showed increased binding to Ca^{2+}-S100A11 compared to the wild-type annexins. This could arise from the substitution of a polar amino acid with

a small hydrophobic residue that might improve peptide−protein contacts. For example, both Met2 and Ser4 are positioned to make contacts with residues in helix I′ (Ile14′) and helix IV (Phe91) and the linker region (Ala45, Asn49), respectively, based on the Ca^{2+}-S100A11/annexin A1 crystal structure. Alternatively, the alanine substitutions at positions 2 (M2A, T2A,) and 4 (S4A, H4A) might act to promote the coil−helix transition and stabilize the α-helical structure of the annexin peptide when bound to S100A11.

In addition to the similar response at positions 2 and 4, the peptide array experiment showed diminished signals at position 6 (F6A, I6A) and especially position 7 (L7A) indicative of reduced interactions with Ca^{2+}-S100A11 with both annexins A1 and A2 upon alanine substitution. This is consistent with the Ca^{2+}-S100A11/annexin A1 structure which shows that Phe6 makes contact with the side chains of residues in helix IV (Cys87 and Ser90) while Leu7 interacts with helix I′ (Glu7′ and Ile10′) of one monomer, and the linker (Leu43, Ala45, and Phe46) and helix IV (Leu83 and Cys87) of the other monomer. In a Ca^{2+}-S100A11/annexin A2 complex, comparison with the S100A10/annexin A2 structure shows that Ile6 and Leu7 would make nearly identical contacts, while Ile6 has additional contacts with Phe90 in helix IV.

The largest differences between the binding of the annexin A1 and A2 peptides to Ca^{2+}-S100A11 was found at positions 3 and 10. For annexin A1 the V3A substitution made little difference to the binding whereas a significant decrease was observed for the V3A annexin A2 peptide, a similar result to that previously observed for the interaction of annexin A2 with S100A10 (*26*). The array also showed that annexin A2 could not tolerate a substitution to alanine at position 10 (L10A) where binding is significantly reduced. In contrast, position 10 is naturally occupied by alanine in annexin A1 in the wild-type sequence. These results clearly indicate that positions 3 and 10 must be occupied by larger hydrophobic residues in annexin A2 but can accommodate smaller hydrophobic residues for annexin A1 for binding to Ca^{2+}-S100A11.

Enhanced binding for K8A and W11A of annexin A1 to Ca^{2+}-S100A11 was observed. Since Lys8 does not directly interact with the S100 protein, the increase in binding may be a result of decreasing hydrophobic side chain (βCH_2-βCH_2) exposure, making the system more entropically favorable. The increased binding of W11A is surprising given its interactions with Phe46, Val55, and Gln50 in the Ca^{2+}-S100A11/annexin A1 complex. Since the more substantial of these contacts are made by Trp11 βCH_2, it may be that substitution by alanine can preserve these interactions. The extreme C-termini of annexin A1 and annexin A2 are affected differently by alanine substitution. For example, in annexin A1 the F12A and D14A peptides have decreased affinity for Ca^{2+}-S100A11 whereas E13A and G14A substitutions in annexin A2 have increased binding. These residues are not observed in the crystal structures of either S100/annexin complex (*18*, *30*).

Identification of Binding Surfaces and Conformation for the Annexin A2 Peptide. The peptide array experiments identified that the N-terminus of annexin A2 interacts with S100A11 in a calcium-sensitive manner. In order to identify the location of the annexin A2 binding surface on the structure of Ca^{2+}-S100A11, chemical shift perturbation experiments were used. These experiments allowed the residues of the S100A11 protein involved in peptide interactions to be identified and compared to residues important for the annexin A1 interaction. Our experiments utilized a modified form of S100A11 where Cys9 was replaced by Ser9, S100A11(C9S). This was done to alleviate oxidation of S100A11, especially during calcium additions that lead to heterogeneous doubling of peaks in NMR spectra, even in the presence of DTT as a reducing agent. This was likely due to a population of the protein forming a Cys9−Cys9 intermolecular disulfide bond that has been observed in the crystal structure of Ca^{2+}-S100A11/annexin A1 (*30*). The resulting S100A11(C9S) mutant had better spectral properties, providing homogeneous $^1H-^{15}N$ HSQC spectra where chemical shift changes could be easily monitored.

The $^1H-^{15}N$ HSQC spectra of Ca^{2+}-S100A11 in the absence and presence of the annexin A2 peptide are shown in Figure 3. There are a large number of chemical shift changes of the amide peaks when the two spectra are compared, indicating that the annexin A2 peptide is binding to the calcium-bound form of S100A11. In contrast, addition of excess annexin A2 peptide to apo-S100A11 resulted in a $^1H-^{15}N$ HSQC spectrum (see Figure S1 in Supporting Information) that was nearly identical to the apo-S100A11 spectrum alone (*42*). This shows that annexin A2 does not bind to the apoprotein. Further, it indicates that calcium binding to S100A11 is required to expose residues (*43*) important for the annexin A2 interaction that, like annexin A1, binds to S100A11 in a calcium-sensitive manner.

To locate the binding site for annexin A2, backbone assignments of S100A11 in the calcium- and annexin A2-bound forms were completed using triple resonance NMR techniques. Of the 97 non-proline residues in the protein, 93 were assigned for Ca^{2+}-S100A11 and 94 for Ca^{2+}-S100A11/annexin A2 (Figure 3). Analysis of the backbone assignments of the calcium- and peptide-bound forms of the S100A11 showed that several of the $^1H-^{15}N$ HSQC peaks exhibited changes in position when the peptide was added to the NMR sample. However, residues that exhibited chemical shift changes greater than the mean change (0.17 ppm) were restricted to residues in helix I (Thr4−Arg8, Ser12−Phe17), the linker (Asn40, Glu42−Lys51), and helix IV (Gln74, Leu77−Ile80, Leu83−Val85, Cys87−His88, Phe91−Ala94) of Ca^{2+}-S100A11. These residues were mapped on the surface of the structure of Ca^{2+}-S100A11 to produce a binding surface for the wild-type annexin A2 peptide (Figure 4).

It is clear from this analysis that there are strong similarities between the binding surface for the Ca^{2+}-S100A11/annexin A2 complex and those observed in the Ca^{2+}-S100A11/annexin A1 and S100A10/annexin A2 structures, respectively (Figure 4). For example, the major cleft used by both S100A10 and S100A11 for annexin A2 and A1 binding is preserved in the annexin A2 surface used by Ca^{2+}-S100A11. In addition, annexin A2 adopts an α-helical structure comprising residues Val3−Asp14 (see Figure S2 in the Supporting Information), the similar structure used by annexin A1 upon binding to Ca^{2+}-S100A11. When the annexin A2 peptide is modeled as an α-helix on this surface and subjected to steepest descents energy minimization, it shows interactions for residues Ile6 with Cys87 and Ser90, Leu7 with Leu43, Ala45, Phe46, and Leu83, and Leu10 with

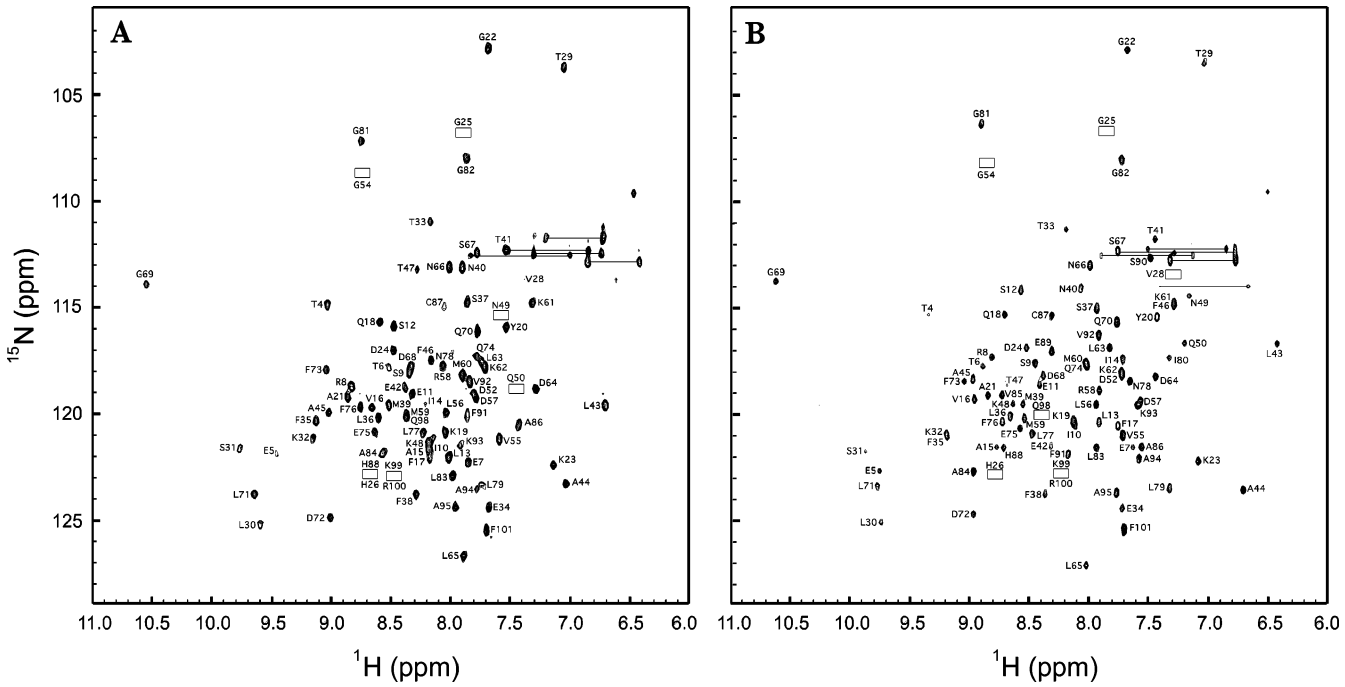

FIGURE 3: ^{1}H−^{15}N HSQC spectra of calcium-bound and calcium−peptide-bound S100A11. (A) ^{1}H−^{15}N HSQC spectrum of 1 mM S100A11-(dimer) in 10 mM $CaCl_2$. (B) ^{1}H−^{15}N HSQC spectrum of 1 mM S100A11(dimer) and 2 mM annexin A2 peptide (Ac-STVHEILSLKQLEGD) under identical conditions as in (A). Both samples also contained 50 mM KCl, 20 mM MOPS buffer, 5 mM DTT, and 90% H_2O/10% D_2O at pH 7.25. Peaks are labeled according to their one-letter amino acid code and residue number. Boxes indicate peaks that are visible at a lower contour level. Tie lines indicate pairs of NH_2 correlations for Asn and Gln residues (not assigned). Spectra were collected on a Varian 600 MHz spectrometer at 35 °C using DSS (0 ppm) as the internal standard.

Phe46, Leu83, Ala86, and Ser90 in Ca^{2+}-S100A11 (Figure 4C,D). In this model residues Ile6 and Leu7 in annexin A2 have either identical or similar contacts as those observed for S100A10. This substantiates the importance of these residues observed in peptide array experiments.

Differences occur for interactions at the C-termini of the annexin A1 and A2 peptides with S100A10 and S100A11. In the energy-minimized Ca^{2+}-S100A11/annexin A2 model (Figure 4C,D) Leu10 in annexin A2 makes contacts with Phe46, Leu83, Ala86, and Ser90. This correlates well with the decrease in binding of annexin A2 to Ca^{2+}-S100A11 observed for the L10A substrate in our peptide array experiments. In contrast, these contacts are not possible for annexin A1 where position 10 is occupied by a much shorter alanine side chain. In annexin A1, the Trp11 and Phe12 positions likely facilitate binding to S100A11 via interactions with Phe46, Val55, and Met59 (Figure 4A) that do not exist in the annexin A2 complexes (Figure 4B,C). Oddly, we observed only a modest chemical shift change for residue Ile10 in Ca^{2+}-S100A11 upon annexin A2 binding. This is surprising since this residue is tightly associated with Val3 in annexin A1 in the Ca^{2+}-S100A11/annexin A1 structure. Since our peptide array experiments showed that Val3 is important in the annexin A2 interaction with Ca^{2+}-S100A11, we feel the small changes in chemical shift observed for Ile10 during annexin A2 binding are a result of its deeply buried amide that is hydrogen bonded to Thr6 in helix I and is insensitive to annexin A2 binding.

Annexin A2 Has Tighter Binding to Ca^{2+}-S100A11 Than Annexin A1. While both the peptide array and chemical shift perturbation experiments indicated calcium-specific binding of annexin A2 to S100A11, it was important to determine that this interaction occurred at a biologically relevant affinity and lifetime. The affinity of annexin A1 for S100A11 was measured by isothermal titration calorimetry by adding Ca^{2+}-S100A11 (10 μL increments) to an annexin A1 peptide solution. Fitting of these data to a single-site binding model provided a dissociation constant of 15.2 ± 0.4 μM, similar to a previous report that showed the binding of annexin A1 to Ca^{2+}-S100A11 had a K_d ~15 μM (*44*).

The dissociation constant for the interaction of Ca^{2+}-S100A11 with annexin A2 could not be determined by calorimetry due to small observed changes in the heat of reaction, leading to inaccurate measurements. Instead, this dissociation constant was determined through titration of the annexin A2 peptide into a sample of Ca^{2+}-S100A11 and monitoring this by NMR spectroscopy. The resulting ^{1}H−^{15}N HSQC spectra indicated that most residues broadened and disappeared during the titration and then reappeared later on, indicative of intermediate exchange on the NMR time scale. Included in this group was Leu43, which changed significantly in both ^{1}H and ^{15}N chemical shift and seemed to undergo pure intermediate exchange, with the initial peak broadening and disappearing into the noise of the spectrum halfway through the titration. For this residue, the ^{1}H frequency difference between the free and bound peaks was about 150 Hz, indicating the off-rate was ~150 s^{-1}. Using this k_{off} as an estimate, close examination of the spectra showed a few resonances such as Ala21, Lys23, Glu34, Met39, Asn66, and Asp72 that shifted by ≪150 Hz, with smaller effects on peak intensity (Figure 5A). For each of these residues the normalized change in chemical shift for each point in the titration was plotted versus peptide concentration, and all six sets of data were globally fit to determine a dissociation constant of 3.3 ± 0.6 μM for annexin A2 binding to Ca^{2+}-S100A11 (Figure 5B).

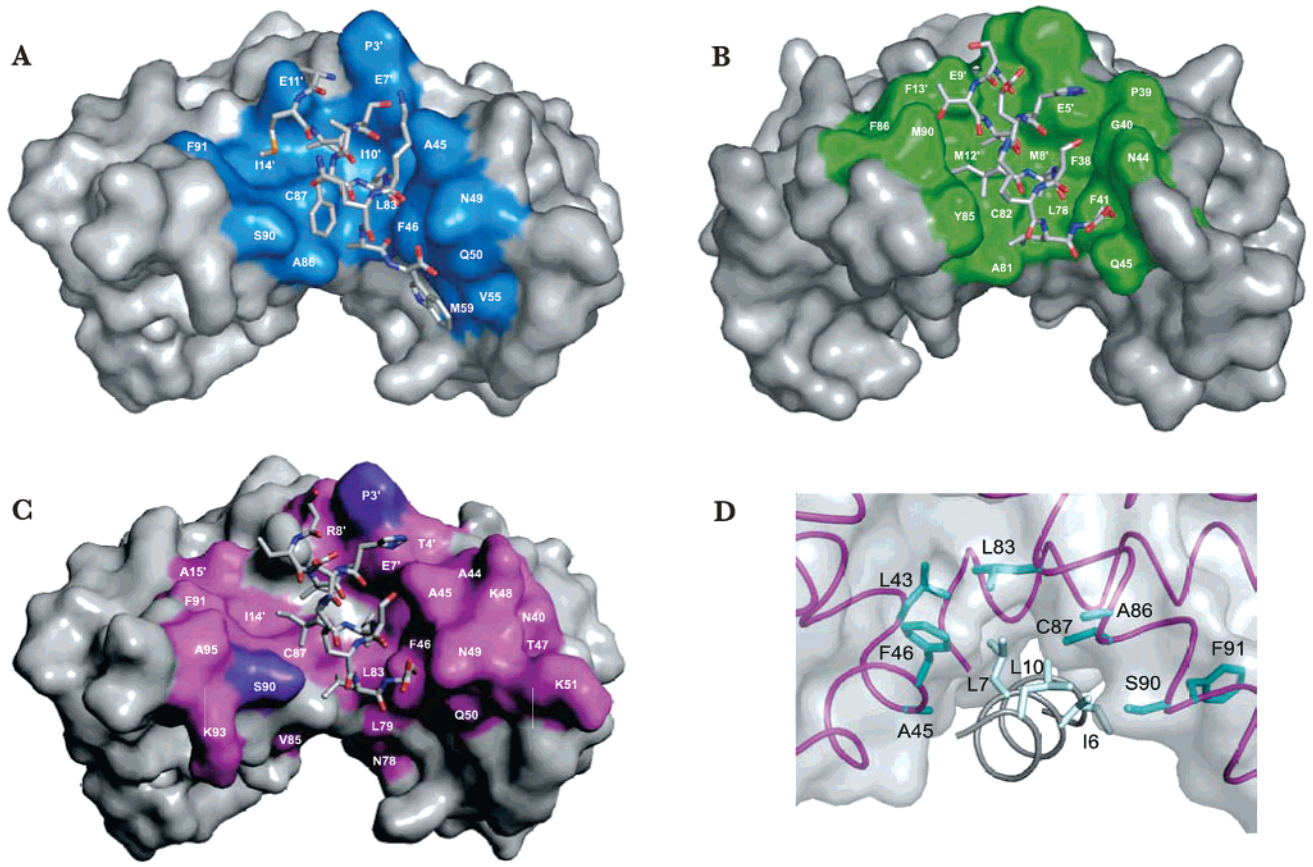

FIGURE 4: Binding surfaces for annexin A1 and A2 on Ca^{2+}-S100A11. (A) Surface representation of the structure of Ca^{2+}-S100A11 bound to annexin A1. The S100A11 residues whose side chains are within 6 Å of the annexin A1 peptide are shaded in blue. The annexin A1 peptide is shown as a stick model. (B) Surface representation of the structure of S100A10 bound to annexin A2 using the same criteria as in (A). (C) A model of the Ca^{2+}-S100A11/annexin A2 complex. This model was generated by superimposing the structures of the Ca^{2+}-S100A11/annexin A1 and S100A10/annexin A2 complexes, followed by the removal of the S100A10 protein and annexin A1 peptide. The resulting complex of Ca^{2+}-S100A11/annexin A2 was then subjected to energy minimization for all residues in the annexin peptide and all residues in the S100A11 structure where significant chemical shifts were observed in the NMR titration. Residues that changed in chemical shift greater than the average change in chemical shift of 0.17 ppm upon peptide binding are highlighted in magenta. Residues Pro3′ and Ser90 are shaded in purple due to the lack of an amide proton or missing assignment, respectively. (D) Energy-minimized Ca^{2+}-S100A11/annexin A2 model showing the interactions of side chains at positions Ile6, Leu7, and Leu10 in annexin A2 (gray helix, pale blue side chains) with residues in Ca^{2+}-S100A11 (magenta helices, cyan side chains). This orientation was created by horizontally rotating the structure shown in (C) by approximately 90°. Residues are labeled according to their one-letter amino acid code and residue number (rabbit S100A11 sequence).

In addition to the dissociation constants for the S100A11/annexin complexes, the lifetime of the Ca^{2+}-S100A11/annexin A2 complex ($\tau = 1/k_{off}$) was determined from the NMR titration data. Using the calculated value for the K_d (Figure 5B), the intermediate exchange NMR data were fit using line shape analysis to determine values for k_{off}. One-dimensional traces in the ^1H dimension through the free and bound peaks at each titration point (Figure 6A,D) were generated to obtain the experimental line shapes of the peaks. This was done for Leu43 (Figure 6B), and the traces were globally fit (Figure 6C) to give a value for k_{off} of 124.6 ± 7.3 s^{-1}. A similar approach for residue Gly69 that appeared to undergo fast-intermediate exchange (Figure 6D) provided a k_{off} of 123.6 ± 6.4 s^{-1} (Figure 6E,F).

DISCUSSION

In the current study, a new interaction between the N-terminus of annexin A2 and Ca^{2+}-S100A11 was identified using peptide array and NMR experiments. The results indicate that the affinity of Ca^{2+}-S100A11 for annexin A2 is nearly 5 times stronger than that of a previously identified target, annexin A1. Further, the dissociation constants for annexin A1 (15.2 ± 0.4 μM) and A2 (3.3 ± 0.6 μM) with Ca^{2+}-S100A11 are in the same range as observed for other S100 complexes. For example, dissociation constants for S100−peptide complexes such as 0.27 ± 0.03 μM for Ca^{2+}-S100B/TRTK-12 (*45*), 23.5 ± 6.6 μM for Ca^{2+}-S100β/p53 (*46*), and 1.6 mM for S100A6/annexin A11 (*10*) association have been previously measured. It is interesting that earlier fluorescence experiments uncovered only nonspecific interactions between Ca^{2+}-S100A11 and an annexin A2 peptide labeled with Prodan at Cys8 (*30*). It is possible that the use of this fluorescent tag perturbed the S100A11/annexin A2 interface, making an interaction difficult to observe. Indeed, our results show that position 8 in annexin A1 is sensitive to substitutions for S100A11 binding. Nevertheless, it is clear from the current work that both N-termini of annexins A1 and A2 interact with S100A11 in a calcium-sensitive manner. This places S100A11 in a group of S100 proteins that includes S100A1 (*47*, *48*) and S100A6 (*9*−*16*) that have been shown to interact with multiple annexin proteins.

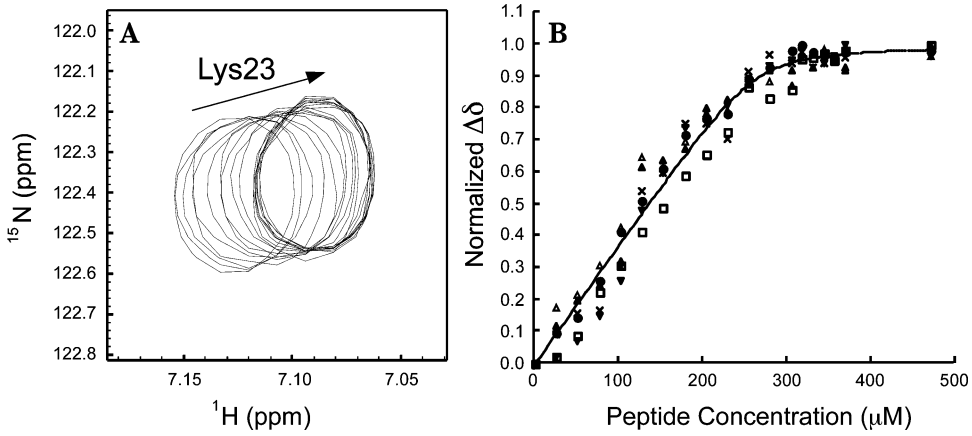

FIGURE 5: Titration of Ca^{2+}-S100A11 with annexin A2 peptide. (A) An overlay from the $^{1}H-^{15}N$ HSQC spectra showing the effect of titrating the annexin A2 peptide into 146.5 μM Ca^{2+}-S100A11(dimer). Small aliquots of the annexin A2 peptide were added to a sample of Ca^{2+}-S100A11, and $^{1}H-^{15}N$ HSQC spectra were collected at each point. Lys23 is an example of a residue that is near the fast exchange limit, where the peak changed only in chemical shift and minimally in line width. The arrow indicates the direction of peak movement during the titration from 0 to 469 μM annexin A2 peptide. (B) Normalized plot of chemical shift change ($\Delta\delta$) versus peptide concentration for fast exchanging residues. The six data sets for Ala21 (▲), Lys23 (●), Glu34 (▼), Met39 (□), Asn66 (△), and Asp72 (×) were globally fit to determine a common dissociation constant ($K_d = 3.3 \pm 0.6$ μM, 95% CI 2.2−4.5 μM) with the lowest total sum-of-squares residual.

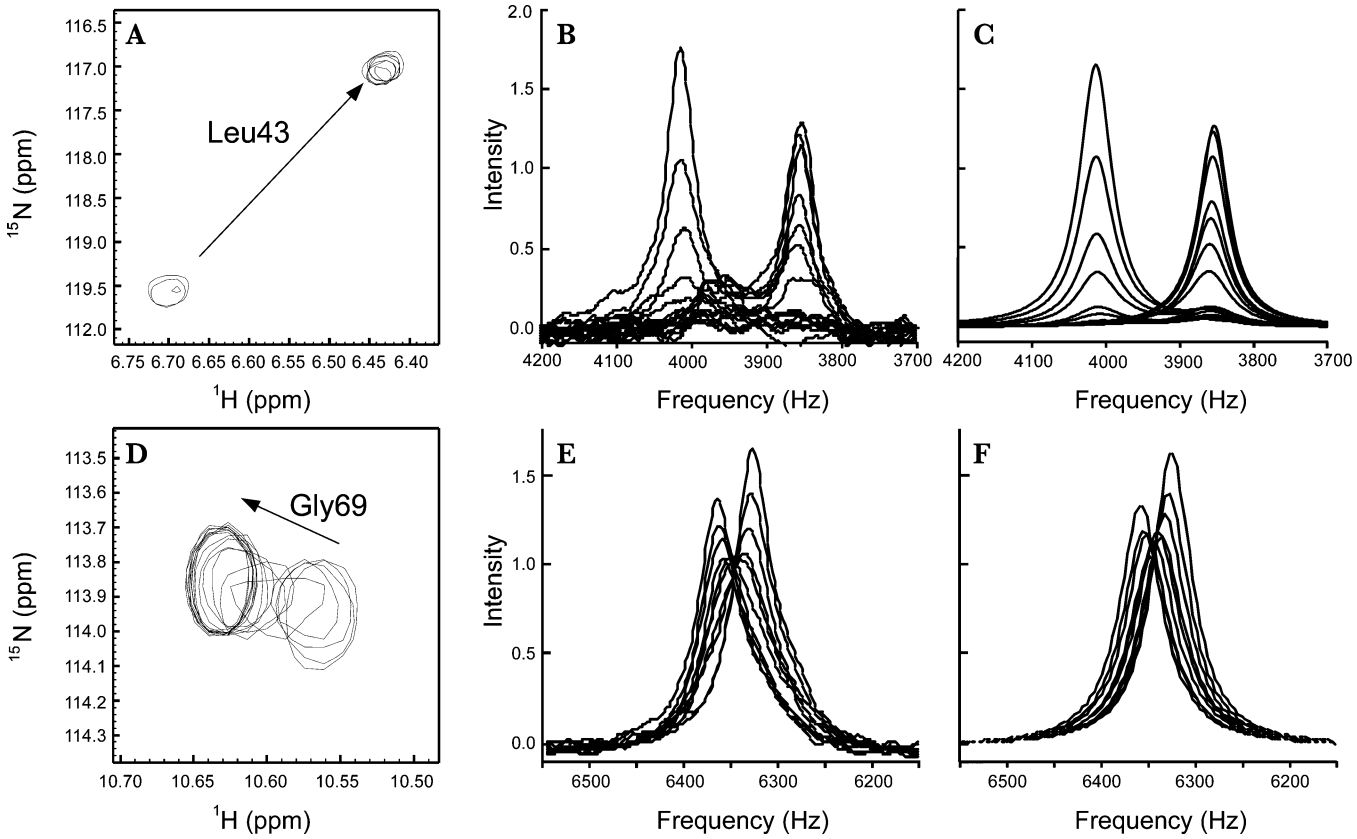

FIGURE 6: Line shape analysis of intermediate exchanging peaks. (A, D) Overlays of regions of the $^{1}H-^{15}N$ HSQC spectra from the annexin A2 titration into Ca^{2+}-S100A11. In (A), Leu43 undergoes intermediate exchange where the peak broadens and disappears during the titration and then reappears in the new position. In (D), Gly69 is an example of fast-intermediate exchange, where the peak changes in chemical shift during the titration and also broadens without completely disappearing. In both cases the arrow indicates the direction of peak movement at increasing annexin A2 concentration. (B, E) One-dimensional ^{1}H traces through the Leu43 and Gly69 peaks at each titration point. (C, F) Line shape analysis of the traces shown in (B) and (E). Each series of peaks was globally fit to determine a value for the off-rate (k_{off}) of the Ca^{2+}-S100A11/annexin A2 complex. The fits yielded $k_{off} = 124.6 \pm 7.3$ s^{-1} (95% CI 110.4−139.0 s^{-1}) for residue Leu43 and $k_{off} = 123.6 \pm 6.4$ s^{-1} (95% CI 111.0−135.9 s^{-1}) for residue Gly69.

S100/annexin complexes such as S100A10/annexin A2 and Ca^{2+}-S100A11/annexin A1 are proposed to facilitate membrane fusion required for membrane vesiculation in events such as endo- and exocytosis (*5*, *8*, *49*). This process requires not only association of the S100/annexin complex but also a calcium-mediated association of the annexin protein with a phospholipid membrane surface. The ability for S100A11 to associate with both annexins A1 and A2 would add a level of diversity to this process. For example, it would allow a single S100 protein to complex with different annexin molecules located at different membrane surfaces. Northern blot analyses for S100A11 (*50*) and

immunohistochemical studies of annexins A1 and A2 (*51*) reveal that this is a distinct possibility since all three proteins are found in placenta, heart, lung, and kidney tissues. This implies that the interactions of annexins A1 and A2 with Ca^{2+}-S100A11 would be mediated by their relative concentrations, the increased affinity of annexin A2 for Ca^{2+}-S100A11, and calcium binding by S100A11.

The k_{off} ($\sim$120 s^{-1}) for the Ca^{2+}-S100A11/annexin A2 complex agrees well with that observed for other calcium-sensor proteins such as calmodulin and troponin C. This is consistent with a signaling role for the association of Ca^{2+}-S100A11 and annexin A2. For example, a k_{off} of 60 s^{-1} has been measured for the calcium-dependent complex between calmodulin and a 43 amino acid peptide derived from adenylate cyclase (*52*). In the case of the muscle contractile protein troponin C, the interaction between its regulatory domain and a peptide derived from troponin I occurs with a k_{off} near 300 s^{-1} (*53*). The off-rates of the Ca^{2+}-S100A11/annexin A2 complex and of the calmodulin and troponin C complexes are all close to 100 s^{-1}, corresponding to a lifetime of about 10 ms. This places them in the same time scale as the duration for a calcium spike (tens of milliseconds range) required for signaling. In addition, the Ca^{2+}-S100A11/annexin A2 lifetime is near the range observed (20−200 ms) for membrane fusion events observed during exocytosis (*49*, *54*, *55*).

The peptide array results of the newly observed interaction of annexin A2 with Ca^{2+}-S100A11 show strong agreement with its interaction with S100A10 (*26*). A study by Becker et al. (*26*) showed that replacement of the hydrophobic side chains at positions 3, 6, 7, and 10 caused a dramatic decrease in the affinity of annexin A2 peptides for S100A10. In the current work, alteration of these four positions resulted in the most significant decrease in binding of annexin A2 to Ca^{2+}-S100A11. This indicates that the N-terminus of annexin A2 uses similar determinants to bind with high affinity to both S100A10 and Ca^{2+}-S100A11. This recognition site on annexin is different for other S100−annexin complexes. For example, a region comprising Q49−T62 in annexin A11 (*10*, *56*) or within the core domain of annexin A2 (*57*) is required for interaction with S100A6. In other cases, such as annexin A6, which can form calcium-sensitive complexes with both S100A1 and S100A6, an obvious 3, 6, 7, 10 hydrophobic pattern does not exist at the extreme N-terminus, suggesting it is another portion of the protein responsible for S100 interaction.

Although not identical, the surface used by Ca^{2+}-S100A11 for the interaction with annexin A2 is similar to that observed for its interaction with annexin A1. This cleft comprises residues in helix I′, the linker, and helix IV of the protein. The similarity between the Ca^{2+}-S100A11/annexin A1 and S100A10/annexin A2 three-dimensional structures and the surfaces used by Ca^{2+}-S100A11 for both annexins A1 and A2 may indicate that this is a general S100/annexin binding region. In addition, the formation of an amphipathic α-helix appears to be required for the mode of interaction of the annexins (*18*, *30*). These characteristics set them apart from other S100 binding partners such as p53 (*58*), Ndr kinase (*59*), and TRTK-12 (*60*) that have either more polar or less α-helical content and do not bridge both S100 monomers as the annexins do. From the annexin perspective, alanine-scanning experiments indicate that the N-terminal regions from annexins A1 and A2 utilize some similar residue positions for their interaction with Ca^{2+}-S100A11. For example, positions 6 and 7 are required to be Ile/Phe and Leu, respectively. It is interesting that these positions appear to confer specificity for binding of at least one annexin sequence since neither annexin A1 nor annexin A2 can bind to Ca^{2+}-S100A6 where methionine and alanine residues are found in these positions in its binding partner, annexin A11 (*61*). However, differences exist at positions 3 and 10 where annexin A1 can tolerate alanine at both positions whereas annexin A2 requires larger hydrophobes (Val3, Leu10) to facilitate binding and cannot tolerate alanine in either position. We suspect this may result from a balance in hydrophobic residue size between positions 3 and 10 in the annexin sequences and the residues that surround these positions. For example, superposition of the Ca^{2+}-S100A11/annexin A1 structure with that of S100A10/annexin A2 shows that the annexin A1 α-helix is approximately 1.0−1.75 Å closer to the S100 protein than for annexin A2. Thus it favors a smaller alanine residue at position 10 and can accommodate alanine at position 3. Further, in annexin A1, Trp11 and Phe12 positions likely facilitate binding to S100A11 via interactions with Phe46, Val55, and Met59 (Figure 4A) that do not exist in the annexin A2 complexes (Figure 4B,C). In this regard, annexin A11 is more similar to annexin A2 because both possess longer chain hydrophobes (Val, Leu, Met) at positions 3 and 10 and a hydrophilic serine at position 11. Although not exhaustive, this indicates that a delicate relationship for annexin binding exists between positions 3, 6, 7, 10, 11, and 12 in these N-terminal annexin sequences.

ACKNOWLEDGMENT

The authors thank Kathryn Barber (University of Western Ontario) for technical support and Qin Liu for assistance in acquiring NMR data and maintenance of the Biomolecular NMR Facility. We also thank Dr. Michael Walsh (University of Calgary) for providing the S100A11 expression vector and for critical reading of the manuscript. We are grateful to Lewis Kay (University of Toronto) for providing pulse sequences and Frank Delaglio (NMRPipe) and Bruce Johnson (NMRView) for software.

SUPPORTING INFORMATION AVAILABLE

Two additional figures, as described in the text. This material is available free of charge via the Internet at http://pubs.acs.org.

REFERENCES

1. Donato, R. (1986) S-100 proteins, *Cell Calcium 7*, 123−145.
2. Santamaria-Kisiel, L., Rintala-Dempsey, A. C., and Shaw, G. S. (2006) Calcium-dependent and -independent interactions of the S100 protein family, *Biochem. J. 396*, 201−214.
3. Maler, L., Potts, B. C., and Chazin, W. J. (1999) High resolution solution structure of apo calcyclin and structural variations in the S100 family of calcium-binding proteins, *J. Biomol. NMR 13*, 233−247.
4. Maler, L., Sastry, M., and Chazin, W. J. (2002) A structural basis for S100 protein specificity derived from comparative analysis of apo and Ca^{2+}-calcyclin, *J. Mol. Biol. 317*, 279−290.
5. Gerke, V., and Moss, S. E. (2002) Annexins: from structure to function, *Physiol. Rev. 82*, 331−371.

6. Harder, T., and Gerke, V. (1993) The subcellular distribution of early endosomes is affected by the annexin II2p11(2) complex, *J. Cell Biol. 123*, 1119−1132.
7. Mayorga, L. S., Beron, W., Sarrouf, M. N., Colombo, M. I., Creutz, C., and Stahl, P. D. (1994) Calcium-dependent fusion among endosomes, *J. Biol. Chem. 269*, 30927−30934.
8. Seemann, J., Weber, K., and Gerke, V. (1997) Annexin I targets S100C to early endosomes, *FEBS Lett. 413*, 185−190.
9. Zeng, F. Y., Gerke, V., and Gabius, H. J. (1993) Identification of annexin II, annexin VI and glyceraldehyde-3-phosphate dehydrogenase as calcyclin-binding proteins in bovine heart, *Int. J. Biochem. 25*, 1019−1027.
10. Tokumitsu, H., Mizutani, A., Minami, H., Kobayashi, R., and Hidaka, H. (1992) A calcyclin-associated protein is a newly identified member of the Ca^{2+}/phospholipid-binding proteins, annexin family, *J. Biol. Chem. 267*, 8919−8924.
11. Filipek, A., Wojda, U., and Lesniak, W. (1995) Interaction of calcyclin and its cyanogen bromide fragments with annexin II and glyceraldehyde 3-phosphate dehydrogenase, *Int. J. Biochem. Cell Biol. 27*, 1123−1131.
12. Filipek, A., and Wojda, U. (1996) p30, a novel protein target of mouse calcyclin (S100A6), *Biochem. J. 320* (Part 2), 585−587.
13. Watanabe, M., Ando, Y., Tokumitsu, H., and Hidaka, H. (1993) Binding site of annexin XI on the calcyclin molecule, *Biochem. Biophys. Res. Commun. 196*, 1376−1382.
14. Minami, H., Tokumitsu, H., Mizutani, A., Watanabe, Y., Watanabe, M., and Hidaka, H. (1992) Specific binding of CAP-50 to calcyclin, *FEBS Lett. 305*, 217−219.
15. Tomas, A., and Moss, S. E. (2003) Calcium- and cell cycle-dependent association of annexin 11 with the nuclear envelope, *J. Biol. Chem. 278*, 20210−20216.
16. Williams, L. H., McClive, P. J., Van Den Bergen, J. A., and Sinclair, A. H. (2005) Annexin XI co-localises with calcyclin in proliferating cells of the embryonic mouse testis, *Dev. Dyn. 234*, 432−437.
17. Semov, A., Moreno, M. J., Onichtchenko, A., Abulrob, A., Ball, M., Ekiel, I., Pietrzynski, G., Stanimirovic, D., and Alakhov, V. (2005) Metastasis-associated protein S100A4 induces angiogenesis through interaction with annexin II and accelerated plasmin formation, *J. Biol. Chem. 280*, 20833−20841.
18. Rety, S., Sopkova, J., Renouard, M., Osterloh, D., Gerke, V., Tabaries, S., Russo-Marie, R., and Lewit-Bentley, A. (1999) The crystal structure of a complex of p11 with the annexin II N-terminal peptide, *Nat. Struct. Biol. 6*, 89−95.
19. Johnsson, N., Marriott, G., and Weber, K. (1988) p36, the major cytoplasmic substrate of src tyrosine protein kinase, binds to its p11 regulatory subunit via a short amino-terminal amphiphatic helix, *EMBO J. 7*, 2435−2442.
20. Osborn, M., Johnsson, N., Wehland, J., and Weber, K. (1988) The submembranous location of p11 and its interaction with the p36 substrate of pp60 src kinase in situ, *Exp. Cell Res. 175*, 81−96.
21. Bianchi, R., Pula, G., Ceccarelli, P., Giambanco, I., and Donato, R. (1992) S-100 protein binds to annexin II and p11, the heavy and light chains of calpactin I, *Biochim. Biophys. Acta 1160*, 67−75.
22. Johnsson, N., and Weber, K. (1990) Alkylation of cysteine 82 of p11 abolishes the complex formation with the tyrosine-protein kinase substrate p36 (annexin 2, calpactin 1, lipocortin 2), *J. Biol. Chem. 265*, 14464−14468.
23. Johnsson, N., and Weber, K. (1990) Structural analysis of p36, a Ca^{2+}/lipid-binding protein of the annexin family, by proteolysis and chemical fragmentation, *Eur. J. Biochem. 188*, 1−7.
24. Harder, T., and Gerke, V. (1994) The annexin II2p11(2) complex is the major protein component of the triton X-100-insoluble low-density fraction prepared from MDCK cells in the presence of Ca^{2+}, *Biochim. Biophys. Acta 1223*, 375−382.
25. Zobiack, N., Gerke, V., and Rescher, U. (2001) Complex formation and submembranous localization of annexin 2 and S100A10 in live HepG2 cells, *FEBS Lett. 500*, 137−140.
26. Becker, T., Weber, K., and Johnsson, N. (1990) Protein-protein recognition via short amphiphilic helices; a mutational analysis of the binding site of annexin II for p11, *EMBO J. 9*, 4207−4213.
27. Kube, E., Weber, K., and Gerke, V. (1991) Primary structure of human, chicken, and *Xenopus laevis* p11, a cellular ligand of the Src-kinase substrate, annexin II, *Gene 102*, 255−259.
28. Kube, E., Becker, T., Weber, K., and Gerke, V. (1992) Protein-protein interaction studied by site-directed mutagenesis. Characterization of the annexin II-binding site on p11, a member of the S100 protein family, *J. Biol. Chem. 267*, 14175−14182.
29. Zokas, L., and Glenney, J. R., Jr. (1987) The calpactin light chain is tightly linked to the cytoskeletal form of calpactin I: studies using monoclonal antibodies to calpactin subunits, *J. Cell Biol. 105*, 2111−2121.
30. Rety, S. D. O., Arie, J.-P., Tabaries, S., Seeman, J., Russo-Marie, F., Gerke, V., and Lewit-Bentley, A. (2000) Structural basis of the Ca^{2+}-dependent association between S100C (S100A11) and its target, the N-terminal part of annexin I, *Structure 8*, 175−184.
31. Naka, M., Qing, Z. X., Sasaki, T., Kise, H., Tawara, I., Hamaguchi, S., and Tanaka, T. (1994) Purification and characterization of a novel calcium-binding protein, S100C, from porcine heart, *Biochim. Biophys. Acta 1223*, 348−353.
32. Grant, G. (2002) *Synthetic Peptides: A User's Guide*, Oxford University Press, New York.
33. Ikura, M., Kay, L. E., and Bax, A. (1990) A novel approach for sequential assignment of ^{1}H, ^{13}C, and ^{15}N spectra of proteins: heteronuclear triple-resonance three-dimensional NMR spectroscopy. Application to calmodulin, *Biochemistry 29*, 4659−4667.
34. Muhandiram, D. R., and Kay, L. E. (1994) Gradient-enhanced triplee-resonance three-dimensional NMR experiments with improved sensitivity, *J. Magn. Reson. 103*, 203−216.
35. Wittekind, M., and Mueller, L. (1993) HNCACB, A high sensitivity 3D NMR experiment to correlate amide proton and nitrogen resonances with the α-carbon and β-carbon resonances in proteins, *J. Magn. Reson., Ser. B 101*, 171−180.
36. Grzesiek, S., and Bax, A. (1992) Correlating backbone amide and side chain resonances in larger proteins by multiple relayed triple resonance NMR, *J. Am. Chem. Soc. 114*, 6291−6293.
37. Delaglio, F., Grzesiek, S., Vuister, G. W., Zhu, G., Pfeifer, J., and Bax, A. (1995) NMRPipe: A multidimensional spectral processing system based on UNIX pipes, *J. Biomol. NMR 6*, 277−293.
38. Johnson, B. A., and Belvins, R. A. (1994) NMRView: A computer program for the visualization and analysis of NMR data, *J. Biomol. NMR 4*, 603−614.
39. Sutherland, I. O. (1971) *The Investigation of the Kinetics of Conformational Changes by Nuclear Magnetic Resonance Spectroscopy*, Vol. 4, Academic Press, London and New York.
40. McConnell, H. M. (1958) Reaction rates by nuclear magnetic resonance, *J. Chem. Phys. 28*, 430−431.
41. Hahn, E. L., and Maxwell, D. E. (1952) Spin echo measurements of nuclear spin coupling in molecules, *Phys. Rev. 88*, 1070−1084.
42. Rintala, A. C., Schonekess, B. O., Walsh, M. P., and Shaw, G. S. (2002) ^{1}H, ^{15}N and ^{13}C resonance assignments of rabbit apo-S100A11, *J. Biomol. NMR 22*, 191−192.
43. Dempsey, A. C., Walsh, M. P., and Shaw, G. S. (2003) Unmasking the annexin I interaction from the structure of Apo-S100A11, *Structure 11*, 887−897.
44. Mailliard, W. S., Haigler, H. T., and Schlaepfer, D. D. (1996) Calcium-dependent binding of S100C to the N-terminal domain of annexin I, *J. Biol. Chem. 271*, 719−725.
45. McClintock, K. A., Van Eldik, L. J., and Shaw, G. S. (2002) The C-terminus and linker region of S100B exert dual control on protein-protein interactions with TRTK-12, *Biochemistry 41*, 5421−5428.
46. Rustandi, R. R., Drohat, A. C., Baldisseri, D. M., Wilder, P. T., and Weber, D. J. (1998) The Ca^{2+}-dependent interaction of S100B (bb) with a peptide derived from p53, *Biochemistry 37*, 1951−1960.
47. Garbuglia, M., Verzini, M., and Donato, R. (1998) Annexin VI binds S100A1 and S100B and blocks the ability of S100A1 and S100B to inhibit desmin and GFAP assemblies into intermediate filaments, *Cell Calcium 24*, 177−191.
48. Garbuglia, M., Verzini, M., Hofmann, A., Huber, R., and Donato, R. (2000) S100A1 and S100B interactions with annexins, *Biochim. Biophys. Acta 1498*, 192−206.
49. Chasserot-Golaz, S., Vitale, N., Umbrecht-Jenck, E., Knight, D., Gerke, V., and Bader, M. F. (2005) Annexin 2 promotes the formation of lipid microdomains required for calcium-regulated exocytosis of dense-core vesicles, *Mol. Biol. Cell 16*, 1108−1119.
50. Inada, H., Naka, M., Tanaka, T., Davey, G. E., and Heizmann, C. W. (1999) Human S100A11 exhibits differential steady-state RNA levels in various tissues and a distinct subcellular localization, *Biochem. Biophys. Res. Commun. 263*, 135−138.

51. Dreier, R., Schmid, K. W., Gerke, V., and Riehemann, K. (1998) Differential expression of annexins I, II and IV in human tissues: an immunohistochemical study, *Histochem. Cell Biol. 110*, 137−148.
52. Craescu, C. T., Bouhss, A., Mispelter, J., Diesis, E., Popescu, A., Chiriac, M., and Barzu, O. (1995) Calmodulin binding of a peptide derived from the regulatory domain of Bordetella pertussis adenylate cyclase, *J. Biol. Chem. 270*, 7088−7096.
53. McKay, R. T., Tripet, B. P., Hodges, R. S., and Sykes, B. D. (1997) Interaction of the second binding region of troponin I with the regulatory domain of skeletal muscle troponin C as determined by NMR spectroscopy, *J. Biol. Chem. 272*, 28494−28500.
54. Albillos, A., Dernick, G., Horstmann, H., Almers, W., Alvarez de Toledo, G., and Lindau, M. (1997) The exocytotic event in chromaffin cells revealed by patch amperometry, *Nature 389*, 509−512.
55. Burgoyne, R. D., and Barclay, J. W. (2002) Splitting the quantum: regulation of quantal release during vesicle fusion, *Trends Neurosci. 25*, 176−178.
56. Sudo, T., and Hidaka, H. (1998) Regulation of calcyclin (S100A6) binding by alternative splicing in the N-terminal regulatory domain of annexin XI isoforms, *J. Biol. Chem. 273*, 6351−6357.
57. Filipek, A., Gerke, V., Weber, K., and Kuznicki, J. (1991) Characterization of the cell-cycle-regulated protein calcyclin from Ehrlich ascites tumor cells. Identification of two binding proteins obtained by Ca2(+)-dependent affinity chromatography, *Eur. J. Biochem. 195*, 795−800.
58. Rustandi, R. R., Baldisseri, D. M., and Weber, D. J. (2000) Structure of the negative regulatory domain of p53 bound to S100B(bb), *Nat. Struct. Biol. 7*, 570−574.
59. Bhattacharya, S., Large, E., Heizmann, C. W., Hemmings, B., and Chazin, W. J. (2003) Structure of the Ca^{2+}/S100B/NDR kinase peptide complex: insights into S100 target specificity and activation of the kinase, *Biochemistry 42*, 14416−14426.
60. McClintock, K. A., and Shaw, G. S. (2003) A novel S100 target conformation is revealed by the solution structure of the Ca^{2+}-S100B-TRTK-12 complex, *J. Biol. Chem. 278*, 6251−6257.
61. Sudo, T., and Hidaka, H. (1999) Characterization of the calcyclin (S100A6) binding site of annexin XI-A by site-directed mutagenesis, *FEBS Lett. 444*, 11−14.

BI061754E